Acta Cryst. (1999). B**55**, 726–735

Synchrotron radiation study of yttria-stabilized zirconia, $Zr_{0.758}Y_{0.242}O_{1.879}$

N. Ishizawa,* Y. Matsushima, M. Hayashi and M. Ueki

Materials and Structures Laboratory, Tokyo Institute of Technology, 4259 Nagatsuta, Midori, Yokohama 226-8503, Japan. E-mail: nishizaw@n.cc.titech.ac.jp

(*Received 27 July 1998; accepted 8 April 1999*)

Abstract

The fluorite-related cubic structure of yttria-stabilized zirconia, $Zr_{0.758}Y_{0.242}O_{1.879}$, has been studied by single-crystal X-ray diffraction using synchrotron radiation and by EXAFS. Two diffraction data sets obtained at X-ray energies of 512 and 10 eV below the Y *K* edge revealed that in the average structure Zr atoms are displaced from the origin of the space group $Fm\bar{3}m$ along ⟨111⟩ by 0.19 Å, while Y atoms reside at the origin. Approximately 48% of the O atoms occupy the ideal position in the fluorite-type structure, while 43% of O atoms are displaced from the ideal position along ⟨001⟩ by 0.31 Å. The remaining 9% of O atoms are presumably sited at interstitial positions. Local structures around Zr and Y are investigated by combining the results of single-crystal X-ray diffraction and EXAFS studies.

1. Introduction

There have been a large number of structural studies of zirconia solid solutions stabilized in a cubic form, because of their importance in industrial applications such as oxygen sensors, solid oxide fuel cells and optical fibre ferules. Here we limit ourselves to those related to the study of the atomic displacements in yttria-doped cubically stabilized zirconia (Y-CSZ) containing ∼10 mol % of Y_2O_3.

The first study for $Zr_{0.74}Y_{0.26}O_{1.87}$ was undertaken by Steele & Fender (1974) using neutron powder diffraction. They reported O-atom displacements of ∼0.36 Å from the ideal positions in the fluorite-type structure and suggested a possible relaxation of metal-atom positions associated with these displacements. Similar results were derived for $Zr_{0.82}Y_{0.18}O_{1.91}$ by single-crystal neutron diffraction (Faber *et al.*, 1978). A single-crystal X-ray diffraction study of $Zr_{0.786}Y_{0.214}O_{1.893}$ revealed that ∼60% of the O atoms are displaced by 0.26 Å along ⟨100⟩, while the remaining O atoms reside at the ideal positions of the fluorite-type structure (Morinaga *et al.*, 1979). However, a single-crystal time-of-flight neutron diffraction study at room temperature on $Zr_{0.724}Y_{0.276}O_{1.862}$ suggested O-atom displacements along ⟨111⟩ rather than ⟨100⟩ (Horiuchi *et al.*, 1984). An X-ray powder diffraction study of $Zr_{0.81}Y_{0.19}O_{1.90}$ using synchrotron radiation, taking advantage of anomalous dispersion afforded by wavelength tunability, suggested different thermal vibration amplitudes between Y and Zr atoms, which were assumed to be sited at the origin (Moroney *et al.*, 1988). The electron diffraction and microscopy studies of $Zr_{0.818}Y_{0.182}O_{1.909}$ (Suzuki *et al.*, 1985, 1987) led to a conclusion similar to that obtained by Faber *et al.* (1978). Three-dimensional profiles of the diffuse scattering of $Zr_{0.61}Y_{0.39}O_{1.805}$ were measured by electron and X-ray diffraction, simulated by the Monte Carlo method, and interpreted in terms of the distribution of oxygen vacancies and associated relaxation of metal-atom positions assuming the ideal positions for O atoms (Welberry *et al.*, 1992, 1993).

Despite these extensive studies, the results do not reach a consensus for Y-CSZ on the magnitude or direction of the displacement of oxygen and metal atoms away from the ideal positions in the fluorite-type structure. This may be partly due to the variety of compositions studied and the various thermal histories of the samples. Since Y-CSZ is essentially metastable at room temperature, it may undergo phase transitions resulting in complex microstructures if annealed for a long time at temperatures where secondary phases nucleate and grow.

Single-crystal studies using integrated intensities of Bragg reflections can only provide information about the 'average structure' in which all unit cells are superimposed. Because of this superposition it is sometimes difficult to detect subtle atomic displacements occurring randomly throughout the crystal. In addition, none of the studies so far have succeeded in measuring respective metal-atom displacements in Y-CSZ because of the experimental difficulty in resolving Y and Zr which have the same number of electrons in the fully ionized states. Such problems can be overcome, in principle, first by enhancing the accuracy of the diffraction data acquisition with the use of synchrotron radiation and second by enhancing the scattering contrast of the atoms of interest, employing wavelengths near the absorption edge.

The present paper describes the average structure of Y-CSZ single crystals grown by the rapid quench method. The yttria composition chosen was close to

10 mol % at which the oxygen-ion transport becomes maximal in the solid solution (Dixon *et al.*, 1963). Two sets of diffraction data were collected using synchrotron radiation at energies far from and just below the Y *K* absorption edge, which enabled us to distinguish between Y and Zr. A spherically shaped small crystal was used to reduce the problems associated with absorption and extinction. As the single-crystal structure analysis does not reveal the local steric configurations around Y and Zr separately, these results were combined with an EXAFS study in order to retrieve chemically plausible local structures around Y and Zr atoms in Y-CSZ.

2. Experimental

2.1. *Sample preparation*

Hf-free $ZrCl_4.nH_2O$ powder (Wako Chemicals Co.) was heated for oxidation at 1473 K for 2 h. The heating process was repeated twice to produce monoclinic ZrO_2. Y_2O_3 powder (99.99% purity, Mitsubishi Chemical Co.) was calcined at 723 K for 24 h. They were then mixed together in an agate mortar with methanol for 1 h. The mixture was heated at 1473 K for 10 h, pulverized and pressed into a rod 1 mm in diameter and 10 mm in length. Crystals were grown using a dual laser-beam heating device (Ishizawa, 1993). The YAG laser beam was split and focused onto the top of the rod through two oppositely faced slanted lenses, causing the top to melt. To prepare single crystals the melt was quenched by closing a shutter inserted along the beam path. Transparent and colourless blocks about 50–100 μm in size were produced and confirmed as single-crystal domains using both a Weissenberg camera and a four-circle diffractometer. A block was then ground into a sphere 35 μm in diameter for the synchrotron radiation diffraction experiment.

2.2. *Synchrotron radiation diffraction*

The diffraction experiment was carried out using a horizontal-type four-circle diffractometer at the beamline 14 A, Photon Factory KEK, which is equipped with a Si (111) double-crystal monochromator and a focusing mirror (Satow & Iitaka, 1989). Two wavelengths 0.7502 and 0.7281 Å, corresponding to the energies 512 and 10 eV below the Y *K* absorption edge of 17038 eV (Sasaki, 1990), were employed. The X-ray energy was calibrated by measuring the EXAFS profile of the crystal near the Y *K* edge. Details of the diffraction experiment are summarized in Table 1. Hereafter the intensity data sets taken at the wavelengths of 0.7502 and 0.7281 Å are referred to as the far-edge and near-edge data sets, respectively.

The cell dimension was determined to be 5.15463 (5) Å at 297 K from 25 reflections in the sin θ/λ range between 0.7759 and 0.9504. The composition x in the formula $(1-x)ZrO_2.xYO_{1.5}$ was determined to be 0.242 (1) from the linear equation in terms of the cell dimension, $a = 0.200x + 5.1063$ (Å), proposed by Yashima *et al.* (1992). The chemical formula of the sample can be written as $Zr_{0.758}Y_{0.242}O_{1.879}$, introducing oxygen vacancies in the fluorite-type formula. All further calculations were carried out assuming this composition. The crystal contains 13.9 mol % of Y_2O_3.

Scattering factors for Y^{3+} and Zr^{4+} were taken from *International Tables for Crystallography* (1992, Vol. C), and those for O^{2-} were taken from Tokonami (1965). Anomalous dispersion coefficients were taken from Sasaki (1989). The $\Delta f'$ for Y, Zr and O are −3.065, −2.181 and 0.009 at 0.7502 Å, and −6.838, −2.541 and 0.009 at 0.7281 Å. There is a difference of ∼3.8 electrons in the real part of the scattering factor of Y between the data sets taken at 0.7502 and 0.7281 Å. In addition, there is a difference of ∼4.3 electrons in the real part of the scattering factors between Y and Zr for the data set taken at 0.7281 Å. The $\Delta f''$ for Y, Zr and O are 0.555, 0.618 and 0.007 at 0.7502 Å, and 0.525, 0.585 and 0.006 at 0.7281 Å. The $\Delta f'$ and $\Delta f''$ for Zr at 0.7281 Å were obtained by a linear interpolation between those at 0.72 and 0.73 Å. Absorption corrections were applied assuming the crystal to be spherical. In the least-squares procedure based on $|F|$, $1/\sigma^2(|F_o|)$ was used as a weight. The isotropic extinction correction was included in the least-squares procedure based on the Becker & Coppens (1974*a*,*b*) formalism. The minimum extinction parameter of 0.88 was observed for the 111 reflection, being large enough to validate the correction. No significant alteration was observed between the difference-Fourier maps calculated after the least-squares procedure with and without the extinction correction. The *Xtal* program package (Hall *et al.*, 1995) was used for structure refinement.

2.3. *EXAFS*

A mixture of Y_2O_3 and ZrO_2 powders was melted in an arc-image furnace (Noma *et al.*, 1989). The melt was quenched and pulverized in a WC mortar.

The EXAFS profiles of the sample near the Y *K* and Zr *K* absorption edges were also measured at beamline 14A of the Photon Factory employing the transmission mode. The range of measurement was 1500 eV with 4 eV steps, starting from 16 740 eV for Y *K* and from 17 699 eV for Zr *K*. The Si (311) double-crystal monochromator was used to tune the energy of X-rays. The EXAFS profiles of Y_2O_3 with the C-type structure (Paton & Maslen, 1965; Maslen *et al.*, 1996) and monoclinic ZrO_2 powders were also measured as references. The measuring time for each step was 3 s. Back-scattering amplitudes were taken from the table given by Teo & Lee (1979).

Table 1. *Experimental details*

	Far-edge set	Near-edge set
Crystal data		
Chemical formula	$Zr_{.758}Y_{.242}O_{1.879}$	$Zr_{.758}Y_{.242}O_{1.879}$
Chemical formula weight	120.73	120.73
Cell setting	Cubic	Cubic
Space group	$Fm\bar{3}m$	$Fm\bar{3}m$
a (Å)	5.15463 (5)	5.15463 (5)
V (Å^3)	136.960	136.960
Z	4	4
D_x (Mg m^{-3})	5.855	5.855
Radiation type	Synchrotron radiation	Synchrotron radiation
Wavelength (Å)	0.7502	0.7281
$\Delta f'$ for Y	−3.065	−6.838
$\Delta f''$ for Y	0.555	0.525
Scan width (°) in ω	0.80	1.0
No. of reflections for cell parameters	0	25
θ range (°)	–	34.40–43.79
μ (mm^{-1})	7.71	7.12
Temperature (K)	293	293
Crystal radius (mm)	0.0175 (5)	0.0175 (5)
Crystal colour	Colourless	Colourless
Data collection		
Diffractometer	Horizontal-type four-circle	Horizontal-type four-circle
Data collection method	Continuous $\theta/2\theta$ scan	Continuous $\theta/2\theta$ scan
Absorption correction	Spherical	Spherical
T_{min}	0.8181	0.8307
T_{max}	0.8229	0.8350
No. of measured reflections	2277	1258
No. of independent reflections	83	90
No. of observed reflections	83	90
Criterion for observed reflections	$F > 3\sigma(F)$	$F > 3\sigma(F)$
R_{int}	0.018	0.018
θ_{max} (°)	68.69	69.8
Range of h, k, l	$-12 \rightarrow h \rightarrow 12$	$-13 \rightarrow h \rightarrow 13$
	$-12 \rightarrow k \rightarrow 12$	$-13 \rightarrow k \rightarrow 13$
	$-12 \rightarrow l \rightarrow 12$	$-8 \rightarrow l \rightarrow 12$
No. of standard reflections	6	6
Frequency of standard reflections	Every 100 reflections	Every 100 reflections
Intensity decay	None	None
Refinement		
Refinement on	F	F
R	0.005	0.009
wR	0.009	0.013
S	6.184	5.876
No. of reflections used in refinement	83	90
No. of parameters used	10	10
Weighting scheme	σ	σ
$(\Delta/\sigma)_{max}$	0	0
$\Delta\rho_{max}$ (e Å^{-3})	0.282	0.286
$\Delta\rho_{min}$ (e Å^{-3})	−0.337	−0.459
Extinction method	Becker & Coppens (1974*a*,*b*)	Becker & Coppens (1974*a*,*b*)
Extinction coefficient	197 (52) $\times 10^1$	198 (22) $\times 10^1$
Computer programs		
Data reduction	*Xtal DIFDAT ABSORB SORTRF ADDREF* (Hall *et al.*, 1995)	*Xtal DIFDAT ABSORB SORTRF ADDREF* (Hall *et al.*, 1995)
Structure solution	*Xtal* (Hall *et al.*, 1995)	*Xtal* (Hall *et al.*, 1995)
Structure refinement	*Xtal CRYLSQ* (Hall *et al.*, 1995)	*Xtal CRYLSQ* (Hall *et al.*, 1995)
Preparation of material for publication	*Xtal BONDLA CIFIO* (Hall *et al.*, 1995)	*Xtal CIFIO* (Hall *et al.*, 1995)

Table 2. *Structure parameters of YSZ crystal based on various models with e.s.d.s in parentheses*

		Ideal fluorite model		Y-shift model		Zr-shift model		Interstitial oxygen model	
		Far-edge	Near-edge	Far-edge	Near-edge	Far-edge	Near-edge	Far-edge	Near-edge
	R	0.0330	0.0389	0.0139	0.0276	0.0130	0.0126	0.0050	0.0090
	wR	0.0672	0.0741	0.0120	0.0390	0.0106	0.0138	0.0092	0.0133
	S	44 (3)	32 (2)	8.0 (7)	17 (1)	7.1 (6)	6.1 (5)	6.2 (5)	5.9 (5)
	ρ_{max} (e Å^{-3})	2.21	1.24	0.18	3.43	0.16	0.33	0.28	0.28
	ρ_{min} (e Å^{-3})	−2.96	−3.88	−1.03	−1.76	−0.99	−0.82	−0.34	−0.46
Zr	x	0	0	0	0	0.0211 (1)	0.0219 (1)	0.02103 (9)	0.0219 (1)
	y	0	0	0	0	$= x$	$= x$	$= x$	$= x$
	z	0	0	0	0	$= x$	$= x$	$= x$	$= x$
	u (Å^2)	0.0179 (4)	0.0193 (3)	0.0142 (1)	0.0169 (2)	0.0087 (2)	0.0101 (2)	0.0086 (2)	0.0100 (2)
Y	x	Same as Zr	Same as Zr	0.0287 (3)	0.0269 (9)	0	0	0	0
	y			$= x$	$= x$	0	0	0	0
	z			$= x$	$= x$	0	0	0	0
	u (Å^2)			0.0049 (4)	0.0001 (12)	0.0059 (1)	0.0005 (2)	0.0059 (1)	0.0006 (2)
O1	x	1/4	1/4	1/4	1/4	1/4	1/4	1/4	1/4
	y	$= x$	$= x$	$= x$	$= x$	$= x$	$= x$	$= x$	$= x$
	z	$= x$	$= x$	$= x$	$= x$	$= x$	$= x$	$= x$	$= x$
	u (Å^2)	0.029 (1)	0.030 (1)	0.016 (2)	0.020 (6)	0.015 (2)	0.019 (2)	0.016 (2)	0.019 (2)
	Pop	0.9395	0.9395	0.43 (9)	0.6 (2)	0.42 (8)	0.53 (8)	0.45 (8)	0.55 (8)
O2	x	None	None	0.311 (5)	0.32 (1)	0.310 (4)	0.317 (5)	0.311 (5)	0.317 (5)
	y			1/4	1/4	1/4	1/4	1/4	1/4
	z			$= y$	$= y$	$= y$	$= y$	$= y$	$= y$
	u (Å^2)			0.0169 (6)	0.015 (4)	0.0169 (5)	0.0163 (9)	0.014 (1)	0.014 (2)
	Pop			0.085 (15)	0.06 (4)	0.087 (14)	0.068 (13)	0.067 (15)	0.053 (15)

3. Results

3.1. *Ideal fluorite model*

The fluorite-type structure with space group $Fm\bar{3}m$ is shown in Fig. 1. The initial structure model, hereafter termed the ideal fluorite model, assumes that Zr and Y atoms occupy the 4(a) sites at the origin and its equivalents, and O atoms occupy the 8(c) sites at $\frac{1}{4},\frac{1}{4},\frac{1}{4}$ and its equivalents. The final R and wR factors based on the ideal fluorite model were 0.0330 and 0.0672 for the far-edge data set and 0.0389 and 0.0741 for the near-edge data set, respectively. The structure parameters are listed in Table 2, together with the results based on our subsequently described models.†

There are several peculiarities in the results obtained for the ideal fluorite model. First the displacement parameters for metal and oxygen atoms were generally large. Second the R factors were also large compared to those usually expected for such simple structures. These peculiarities have been common observations thus far for Y-CSZ crystals (see, for example, Morinaga *et al.*, 1979; Horiuchi *et al.*, 1984) and, consequently, the basis for claiming that the structure deviates from the ideal fluorite model.

The difference Fourier maps of the (110) section are shown in Figs. 2(a) and 2(b) for the far-edge and near-edge data sets, respectively. The corresponding section is hatched in Fig. 1. There is an accumulation of excess electrons of ∼0.9 e Å^{-3} along ⟨100⟩ near the O atoms. The topography of residual electron densities around the oxygen site is essentially the same as that reported by Morinaga *et al.* (1979). Hence, we were also led to a similar conclusion that approximately half of the O atoms (O1) occupy the ideal 8(c) sites and most of the

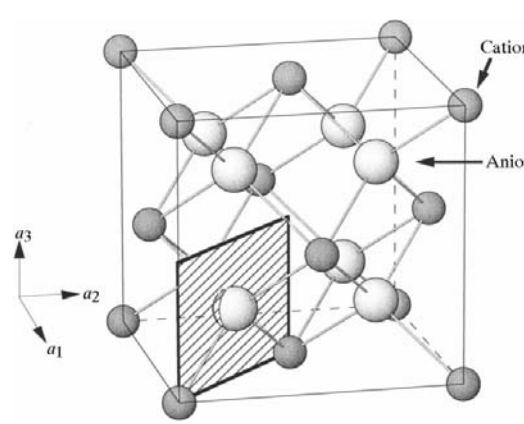

Fig. 1. Fluorite structure. The hatched region corresponds to the difference Fourier section in Fig. 2.

† Supplementary data for this paper are available from the IUCr electronic archives (Reference: OH0066). Services for accessing these data are described at the back of the journal.

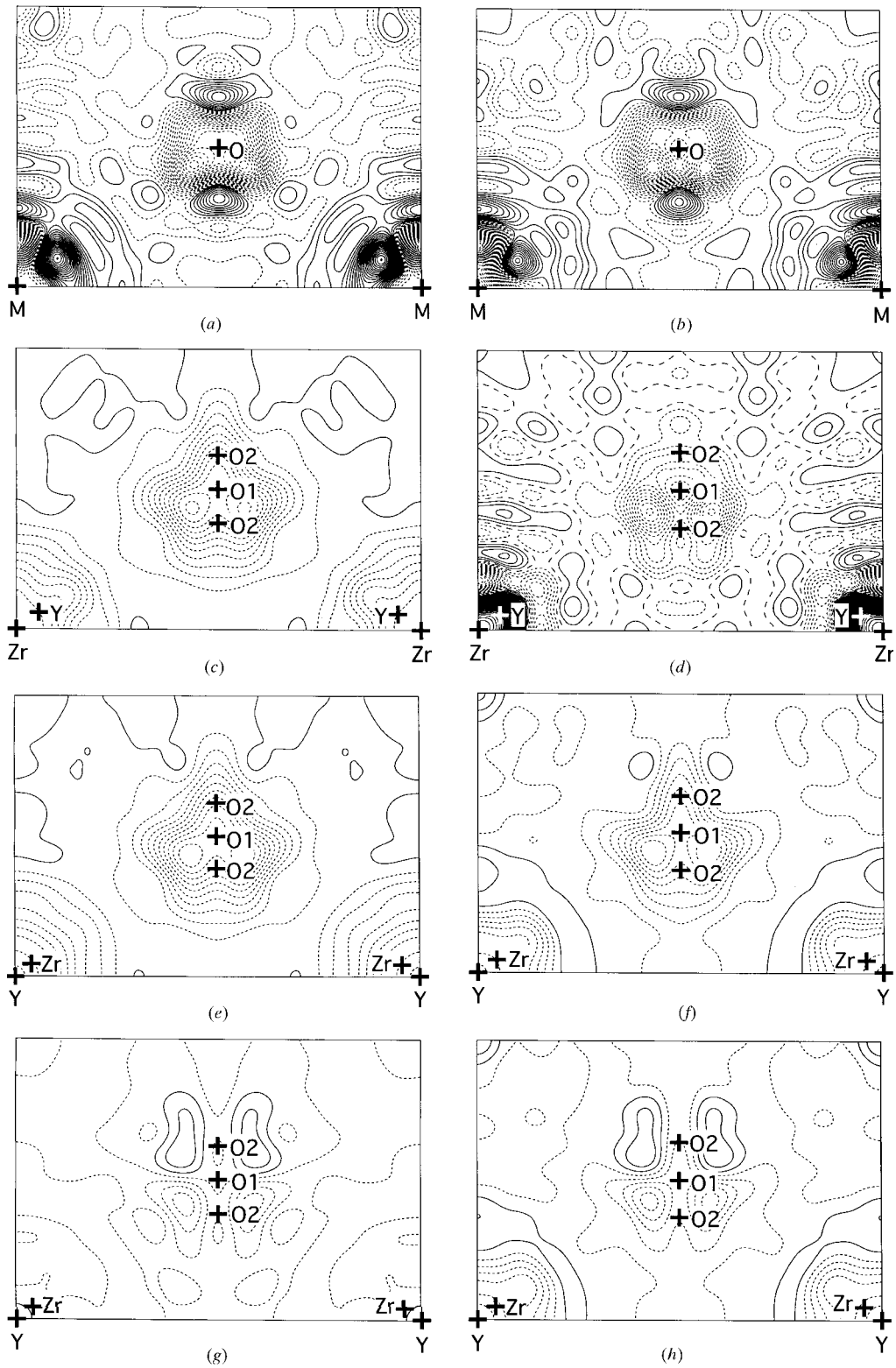

Fig. 2. Difference Fourier maps of the (110) section of Y-CSZ based on (*a*) and (*b*) ideal fluorite models, (*c*) and (*d*) Y-shift models, (*e*) and (*f*) Zr-shift models, and (*g*) and (*h*) interstitial O-atom models, where the former (*a*), (*c*), (*e*) and (*g*) are obtained from the far-edge data set, while the latter (*b*), (*d*), (*f*) and (*h*) from the near-edge data set. The map corresponds to the hatched area in Fig. 1. Map borders 2.577 × 3.645 Å; contour interval 0.1 e $Å^{-3}$; positive, negative contours – solid, short dashes, respectively.

remaining O atoms (O2) occupy the 48(g) sites with x taking a value close to $\frac{1}{4}$.

Another feature in Figs. 2(a) and 2(b) is an accumulation of excess electrons of $\sim$2.2 e Å^{-3} along ⟨111⟩ near the metal atoms, suggesting a possible displacement of metal atoms. It is reasonable to assume that the Zr and Y atoms prefer different steric configurations of neighbours depending on the nature of their bonding. This will result in Y and Zr atoms taking slightly different positions. Therefore, we have investigated two models, one involving a Y shift and the other a Zr shift.

3.2. *Y-shift model*

In this model all the Y atoms are assumed to occupy the 32(f) sites with x taking a value close to 0, while Zr atoms reside at the 4(a) sites. In addition, some of the O atoms (O2) are assumed to occupy the 48(g) sites and the rest of the O atoms (O1) the 8(c) sites. The population parameter was also refined assuming all the O atoms occupy either 48(g) or 8(c) sites.

The refinement terminated with R/wR of 0.0139/0.0120 for the far-edge data set and 0.0276/0.0390 for the near-edge data set. The final parameters are given in Table 2. The difference Fourier maps of the (110) section are shown in Figs. 2(c) and 2(d) for the far-edge and near-edge data sets, respectively.

There are two peculiarities. One is a large difference in R factors between the far-edge and near-edge data sets. The other is the displacement parameter of Y being too small compared with that of Zr. Although the difference Fourier map of Fig. 2(c) obtained for the far-edge data set looks much improved compared with the ideal fluorite model, there still remain large artefacts around the metal atoms in Fig. 2(d) obtained for the near-edge data set.

If the structure model is correct, the resultant difference Fourier maps should give a similar topography for both far- and near-edge data sets. As mentioned in the *Experimental*, however, there is a difference of $\sim$3.8 electrons in the real part of the scattering factor of Y between the far- and near-edge data sets. This may be the reason for the large difference in those maps if the assumed model is incorrect. We concluded that this was the case for the Y-shift model.

3.3. *Zr-shift model*

In this model Zr and Y atoms are assumed to occupy the 32(f) and 4(a) sites, respectively, in a reverse manner to the Y-shift model. The other conditions were assumed to be the same as those for the Y-shift model. The refinement terminated with the final R/wR factors of 0.0130/0.0106 for the far-edge data set and 0.0126/0.0138 for the near-edge data set. The final parameters are given in Table 2. The difference Fourier maps of the (110) section are shown in Figs. 2(e) and 2(f) for the far- and near-edge data sets, respectively.

Displacement parameters for Zr and Y atoms converged to more reasonable values than the corresponding values for the Y-shift model. The residual electron density maps in Figs. 2(e) and 2(f) showed a similar topography, suggesting that the Zr-shift model is superior to the Y-shift model. The accumulation of residual electrons near the metal-atom positions due to artefacts caused by the model inadequacy was reduced in the Zr-shift model (Fig. 2f) compared to the Y-shift model (Fig. 2d) obtained for the same near-edge data set. This is mainly due to the 4.3 electron difference in $\Delta f'$ between Y and Zr of the near-edge data set.

The improvement of the R factor is notable for the near-edge data set. The α factor of the significance test (Hamilton, 1974) for the Zr-shift model with respect to the Y-shift model was less than 0.005 for the near-edge data set. All these results warrant the Zr-shift model. However, a relatively large depletion of electrons near the oxygen positions suggested that there is still room for further improvement by considering the oxygen population in more detail.

3.4. *Interstitial O-atom model*

Populations of atoms O1 at 8(c) and O2 at 48(g) sites were examined. If we assume that all the O atoms occupy either 8(c) or 48(g) sites, the resultant distributions among these sites are 45% for 8(c) and 55% for 48(g). If we remove this constraint and refine the population parameters independently, they become 48% for 8(c) and 43% for 48(g). The remaining 9% of O atoms are presumably sited at interstitial positions. If we write such O atoms at the interstitial positions as OX, the composition of the crystal can then be expressed as $Zr_{0.758}Y_{0.242}O1_{0.900}O2_{0.804}OX_{0.175}$. The refinement terminated with the final R/wR factors of 0.0050/0.0092 for the far-edge data set and 0.0090/0.0133 for the near-edge data set.

The difference Fourier maps of the (110) section are shown in Figs. 2(g) and 2(h) for the far- and near-edge data sets, respectively. No evidence was obtained about the site preference of OX atoms. This may be due to the small number of OX atoms or to the variety of plausible sites that can be occupied. The residual electron densities around the O atoms exhibits a butterfly-shaped topography consisting of electron depletion along metal atoms and accumulation along the 4(b) sites at the top-right and top-left corners of Fig. 2. The 4(b) sites are at the centres of large cages surrounded by eight oxygen atoms in the fluorite-type structure. The accumulation and depletion of electrons near the O atom could be ascribed to the presence of an odd order anharmonic term of the thermal vibration of O atoms, which may facilitate a jump through the large cage of the structure at elevated temperatures. However, in this study it was difficult to analyse the anharmonic terms due to the

Table 3. *Possible bond distances calculated from the average structure of Y-CSZ*

Cation	Oxygen type	Distance (Å) with e.s.d.s in parentheses	Symmetry operation (representative)	Number of equidistant bonds/site multiplicity
Y at origin	O1	2.23202 (1)	x,y,z	8/8
	O2	2.067 (12)	$\frac{1}{2}-x,\frac{1}{2}-y,z$	24/48
	O2	2.426 (16)	x,y,z	24/48
Zr at (x,x,x) $x = 0.02103$	O1	2.0443 (5)	x,y,z	1/8
	O1	2.1766 (5)	$-y,x,z$	3/8
	O1	2.3014 (5)	$x,-y,-z$	3/8
	O1	2.4198 (5)	$-y,-x,-z$	1/8
	O2	1.881 (11)	$\frac{1}{2}-x,\frac{1}{2}-y,z$	3/48
	O2	1.990 (13)	$\frac{1}{2}-y,-\frac{1}{2}+x,z$	3/48
	O2	2.024 (11)	$-z,\frac{1}{2}-y,\frac{1}{2}-x$	6/48
	O2	2.126 (13)	$-\frac{1}{2}+x,y,-\frac{1}{2}+z$	6/48
	O2	2.158 (10)	$\frac{1}{2}-x,-y,-\frac{1}{2}+z$	3/48
	O2	2.240 (16)	x,y,z	3/48
	O2	2.254 (12)	$-y,-\frac{1}{2}+x,-\frac{1}{2}+z$	3/48
	O2	2.361 (16)	$-y,x,z$	6/48
	O2	2.390 (18)	$y,-x,z$	3/48
	O2	2.477 (15)	$x,-y,-z$	3/48
	O2	2.504 (17)	$-x,-y,z$	6/48
	O2	2.613 (16)	$-y,-x,-z$	3/48

presence of many O-atom positions at 48(g) close to 8(c).

The final structural parameters are given in Table 2. All the possible bond distances for Y and Zr are given in Table 3.

3.5. *EXAFS*

The Fourier transforms of the EXAFS oscillation, $\chi(k)$, as a function of the wavenumber k of electrons are shown in Fig. 3 for the Y K edge and Zr K edge, respectively. The transform is weighted by k^3. The phase shifts were not corrected at this stage. The first oxygen shell surrounding Y is located around 1.8 Å and that surrounding Zr is located around 1.6 Å in the figure. The parameter fitting was carried out for the first shells, using a program coded by one of the authors (YM) based on the algorithm given by Udagawa (1993). The R factors between the experimental and calculated EXAFS defined as $\sum(k^3\chi_{\rm exp}-k^3\chi_{\rm calc})^2/\sum(k^3\chi_{\rm calc})^2$ were 0.073 for Y K and 0.069 for Zr K. Results are summarized in Table 4.

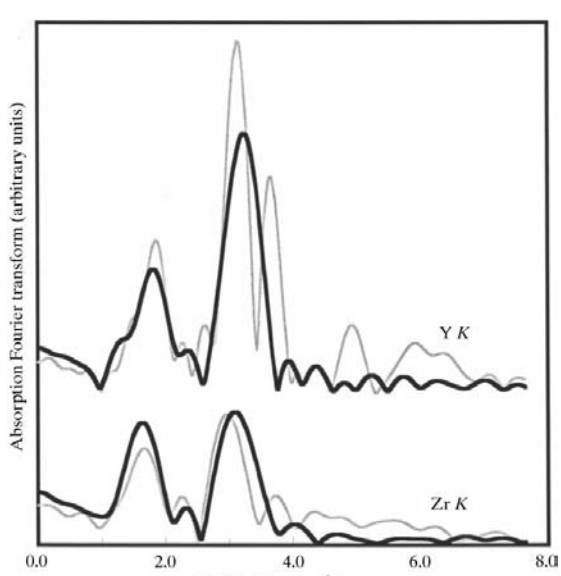

Fig. 3. Fourier transforms of the Y K edge data for Y-CSZ (black line) and C-type Y_2O_3 (grey line) in upper figures and the Zr K edge data for Y-CSZ (black line) and monoclinic ZrO_2 (grey line) in lower figures.

The distance between Y and the first shell is 2.32 (1) Å and that between Zr and the first shell is 2.13 (1) Å, which is consistent with results obtained by the past studies including Catlow *et al.* (1986), Morikawa *et al.* (1988) and Li *et al.* (1993*b*).

The coordination numbers N for Y and Zr atoms are 5.9 (3) and 7.0 (3), respectively. These values fall within the range of values reported by previous EXAFS studies. The diversity of N may be attributed to the high correlation between N and σ, of which the latter represents both thermally induced vibrational displacements and static displacements within a shell of neighbours.

4. Discussion

4.1. *Discrepancy of the ideal fluorite model*

The EXAFS results indicated that the Y—O and Zr—O bond distances are 2.32 (1) and 2.13 (1) Å, respectively. The latter is significantly shorter than the former by 0.19 (1) Å. On the other hand, the ideal fluorite model for the structure allows a single bond distance of

2.232 (1) Å for both Y—O and Zr—O. Therefore, the ideal fluorite model cannot describe the Y-CSZ structure adequately.

A simple calculation of the weighted mean bond distance from Table 3 gives 2.24 (1) Å for both Y—O and Zr—O, assuming that all the available sites for O atoms are partially filled with the refined population values in the interstitial O-atom model. The weighted mean values for Y—O and Zr—O are close to each other and the value obtained for the ideal fluorite model, and largely apart from those expected by the EXAFS study. This suggests that even our final model is also inappropriate in view of bond distance if we take the average. It follows from this that there should be several typical local structure units around Y and Zr which accommodate the dissimilar Y—O and Zr—O mean bond distances revealed by the EXAFS analysis. The average structure can be interpreted in terms of superposition of these units oriented in various crystallographic directions in a crystal.

We discuss below the steric configuration of YO_6 and ZrO_7 as plausible local structure units, with the coordination numbers 6 and 7, respectively, derived from the present EXAFS results. Other coordination numbers, especially higher ones, may be possible for both metal atoms in this compound if we take into consideration the number of oxygen vacancies in the crystal. However, we consider them beyond the scope of this paper partly because such highly coordinated local structures might be obtained simply by locating extra O atoms at far distances without changing seriously the basic geometric configuration of YO_6 and ZrO_7 or from the ideal fluorite model itself.

4.2. *Geometrical configuration of YO_6*

The C-type Y_2O_3 with the space group $Ia\bar{3}$ is stable up to a temperature of ~105 K below its melting point of 2706 K (Yamada *et al.*, 1986). The high-temperature form is commonly believed to be hexagonal (Foex & Traverse, 1966), although the structure has not been determined. There is another report that Y_2O_3 forms a fluorite-type $Fm\bar{3}m$ structure at temperatures near the melting point (Katagiri *et al.*, 1993). The existence of the eight-coordinated Y and Zr atoms in both end members of the Y_2O_3–ZrO_2 system at high temperatures supports the stability of fluorite structure in the Y-CSZ solid solution over a wide composition range at high temperatures. On the other hand, the existence of a six-cordinated Y atom in the C-type Y_2O_3 suggests a possible change in the local structure around Y in Y-CSZ from the fluorite-type to the C-type when the temperature is decreased. In this section a similarity between the local structures around Y in Y-CSZ and the C-type Y_2O_3 at room temperature is described.

There are two crystallographically independent Y1 and Y2 atoms in the C-type Y_2O_3 (Paton & Maslen, 1965; Maslen *et al.*, 1996). They are both surrounded by six O atoms in an almost cubic arrangement with two missing O atoms related by either the body diagonal of the cube (Y1) or the face-diagonal (Y2). These YO_6 polyhedra in Y_2O_3 are depicted in Figs. 4(*a*) and 4(*b*). The ratio of $Y1O_6$ to $Y2O_6$ polyhedra is 1:3 in C-type Y_2O_3. The mean Y—O bond distance is 2.282 Å, which is the same as that observed by EXAFS for the Y—O distance in Y-CSZ, within experimental error. The coordination number of Y in Y-CSZ is inferred by our EXAFS study to be 5.9 (3), which is also close to 6, as observed in C-type Y_2O_3.

Table 4. *EXAFS results*

N: coordination number, *R*: interatomic distance (Å), σ: Debye–Waller factor (Å)

Centre atom	*N*	*R*	σ
Y	5.9 (3)	2.32 (1)	0.064 (3)
Zr	7.0 (3)	2.13 (1)	0.072 (3)

We propose two models for the geometrical configuration of YO_6 in Y-CSZ and these are depicted in Figs. 4(*d*) and 4(*e*). The insets show O-atom positions chosen from the available 8(*c*) and 48(*g*) sites. The model in Fig. 4(*d*) consists of six O1 at 8(*c*) and no O2 at 48(*g*). The configuration corresponds to the $Y1O_6$ polyhedron in C-type Y_2O_3 with the two missing O atoms related by the body diagonal of the cube, as shown in Fig. 4(*a*). The other model shown in Fig. 4(*e*) consists of four O1 at 8(*c*) and two O2 at 48(*g*). This configuration corresponds to $Y2O_6$ in C-type Y_2O_3 with the two missing O atoms related by the face-diagonal of the cube, as shown in Fig. 4(*b*). The mean Y—O distances are 2.232 Å for the YO_6 model in Fig. 4(*d*) and 2.297 Å in Fig. 4(*e*). The mean distances are approximately the same as each other and in accordance with the EXAFS result and those for the $Y1O_6$ and $Y2O_6$ in C-type Y_2O_3.

4.3. *Geometrical configuration of ZrO_7*

ZrO_2 crystallizes from the melt into a cubic form at 2953 K. The crystal then undergoes phase transitions from cubic to tetragonal at 2643 K and from tetragonal to monoclinic at 1443 K. The monoclinic form is stable at room temperature. Hence, the nature of the Zr—O bonding in monoclinic ZrO_2 and resultant geometrical configuration of Zr and its neighbouring O atoms are presumably reflected in the room-temperature structure of Y-CSZ as well.

There are two crystallographically independent OI and OII atoms in monoclinic ZrO_2, following the conventional atom-labelling scheme given by McCullough & Trueblood (1959) and Smith & Newkirk (1965). The ZrO_7 polyhedron in ZrO_2 is depicted in Fig. 4(*c*). The Zr atom is surrounded by three OI and four OII atoms. The four OII atoms form approximately a square,

while the three OI atoms form a distorted triangle almost parallel to the OII square. The bond distances of three Zr—OI range between 2.051 and 2.163 Å with the mean value of 2.090 Å. Those of the four Zr—OII range between 2.151 and 2.285 Å with the mean value of 2.211 Å. The overall mean bond distance for the seven Zr—O bonds is 2.159 Å, which are in accordance with the observed EXAFS Zr—O distance of 2.15 (1) Å in Y-CSZ, within experimental error. The coordination number seven in monoclinic ZrO_2 agrees with 7.0 (3) in Y-CSZ, as determined by EXAFS.

A plausible model for the local structure around Zr in Y-CSZ is depicted in Fig. 4(*f*). The inset shows the shifts of constituent atoms from the ideal fluorite structure. In the model three O1 and four O2 surround the Zr atom, which is displaced along ⟨111⟩. Resultant Zr—O distances are given in the figure. They range from 2.024 to 2.301 Å with the mean value of 2.136 Å both in agreement with the EXAFS result and the distances observed in monoclinic ZrO_2. The presence of the noncentrosymmetric local structure of ZrO_7 in Y-CSZ is consistent with the picture inferred by Li *et al.* (1993*a*,*b*) from their EXAFS studies.

The presence of the ZrO_7 local structure model in Y-CSZ can be ascertained from the results of Raman spectroscopy as well (Yashima *et al.*, 1996). Despite the intrinsic broadening of bands in the Raman spectrum for Y-CSZ due to structural disorder, we can observe similarities between the spectra for monoclinic ZrO_2 and Y-CSZ, and dissimilarities between the spectra for tetragonal ZrO_2 and Y-CSZ. This is well demonstrated, for example, by following a peak around 100 cm^{-1} in Fig. 4 of the paper of Yashima *et al.* (1996) with composition for the system ZrO_2–$YO_{1.5}$. The peak is sharp in monoclinic ZrO_2 with $YO_{1.5}$ content between 0 and 2 mol %, then disappears in the tetragonal region between 6 and 10 mol %, and again becomes notable in the cubic region above 16 mol %.

4.4. *Bond-valence sums*

The expected valence of metal atoms is calculated from the retrieved local structure models using the bond-valence method (Brown & Altermatt, 1985). The valence of Y is calculated to be +3.37 for the YO_6 model in Fig. 4(*d*) and +2.92 for the model in Fig. 4(*e*). If we assume the presence ratio of 1:3 in a similar way for Y_2O_3, the valence becomes +3.03 which is close to the formal charge +3 of Y cations. The valence of Zr atoms in Y-CSZ is calculated to be +4.15 for the ZrO_7 model in Fig. 4(*f*), being also close to the formal charge +4 of the Zr cation.

5. Conclusions

Single-crystal X-ray diffraction data of yttria-stabilized cubic zirconia $Zr_{0.758}Y_{0.242}O_{1.879}$ were collected at two X-ray energies, 512 and 10 eV below the Y *K* edge using

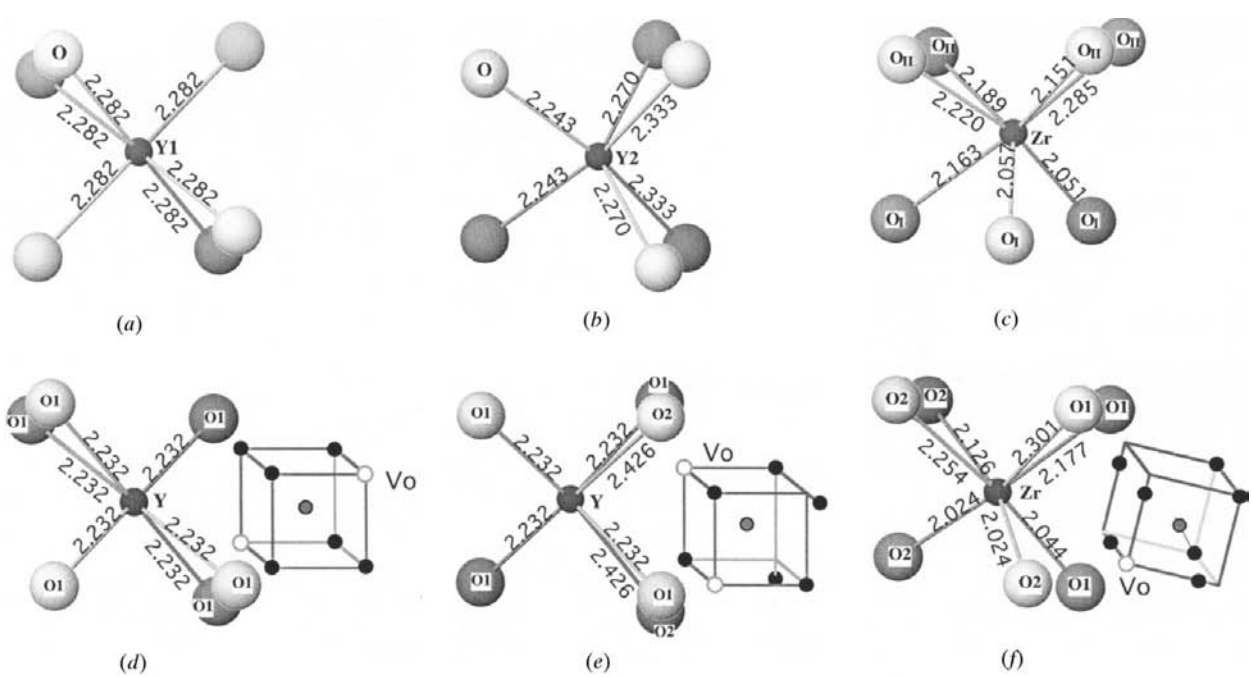

Fig. 4. Schematic view of (*a*) $Y1O_6$ and (*b*) $Y2O_6$ polyhedra in C-type Y_2O_3, (*c*) ZrO_7 polyhedron in monoclinic ZrO_2, (*d*) and (*e*) two YO_6, and (*f*) ZrO_7 local structure models in Y-CSZ with bond distances given in Å. The models (*d*), (*e*) and (*f*) in Y-CSZ geometrically correspond to (*a*), (*b*) and (*c*), respectively. The insets show schematic atom displacements from the cubic coordination polyhedra. Vo is an O-atom vacancy. O atoms near the back face of the cube are shaded darker.

synchrotron radiation. In the fluorite-type structure with the space group $Fm\bar{3}m$, the Y atoms occupy the 4(*a*) sites, whereas the Zr atoms occupy the 32(*f*) sites 0.19 Å apart from the 4(*a*) sites. 48% of the O atoms occupy the 8(*c*) sites and 43% of the O atoms are shifted 0.31 Å along ⟨001⟩ and sited at the 48(*g*) sites. The remaining O atoms are presumably sited at interstitial positions. Typical steric configurations for YO_6 and ZrO_7 similar to those found in C-type Y_2O_3 and monoclinic ZrO_2 were retrieved from the average structure of Y-CSZ as possible candidates for the representative local structures around Y and Zr, respectively, in Y-CSZ.

We wish to thank Professor M. Yoshimura of our Laboratory for allowing us to use his arc image furnace for the EXAFS sample preparation, Professor M. Kakihana of our Laboratory for a discussion about the interpretation of Raman spectra, and Drs J. G. Thompson and R. L. Withers of the Australian National University for helpful comments during the preparation of this manuscript. The synchrotron experiments at KEK were performed based on the programs 93G025 and 95G334.

References

Becker, P. J. & Coppens, P. (1974*a*). *Acta Cryst.* A**30**, 129–147.
Becker, P. J. & Coppens, P. (1974*b*). *Acta Cryst.* A**30**, 148–153.
Brown, I. D. & Altermatt, D. (1985). *Acta Cryst.* B**41**, 244–247.
Catlow, C. R. A., Chadwick, A. V., Greaves, G. N. & Moroney, L. M. (1986). *J. Am. Ceram. Soc.* **69**, 272–277.
Dixon, J. M., LaGrange, L. D., Merten, U., Miller, C. F. & Porter II, J. T. (1963). *J. Electrochem Soc.* **110**, 276–280.
Faber, J. Jr, Mueller, M. H. & Cooper, B. R. (1978). *Phys. Rev. B*, **17**, 4884–4888.
Foex, M. & Traverse, J.-P. (1966). *Rev. Int. Hautes Temp. Refract.* **3**, 429–453.
Hall, S. R., King, G. S. D. & Stewart, J. M. (1995). Editors. *Xtal*3.4 *User's Manual*. University of Western Australia, Lamb, Perth.
Hamilton, W. C. (1974). *International Tables for X-ray Crystallography*, Vol. 4, pp. 288–292. Birmingham: Kynoch Press. (Present distributor Kluwer Academic Publishers, Dordrecht.)
Horiuchi, H., Schultz, A. J., Leung, P. C. W., Williams, J. M. (1984). *Acta Cryst.* B**40**, 367–372.
Ishizawa, N. (1993). Report of RLEM, Vol. 18, pp. 1–7. Tokyo Institute of Technology.
Katagiri, S., Ishizawa, N. & Marumo, F. (1993). *Powder Diffr.* **8**, 60.
Li, P., Chen, I.-W. & Penner-Hahn, J. E. (1993*a*). *Phys. Rev. B*, **48**, 10063–10073.
Li, P., Chen, I.-W. & Penner-Hahn, J. E. (1993*b*). *Phys. Rev. B*, **48**, 10074–10081.
Maslen, E. N., Streltsov, V. A. & Ishizawa, N. (1996). *Acta Cryst.* B**52**, 414–422.
McCullough, J. D. & Trueblood, K. N. (1959). *Acta Cryst.* **12**, 507–511.
Morikawa, H., Shimizugawa, Y., Marumo, F., Harasawa, T., Ikawa, H., Tohji, K. & Udagawa, Y. (1988). *J. Ceram. Soc. Jpn*, **96**, 253–258.
Morinaga, M., Cohen, J. B. & Faber, J. Jr (1979). *Acta Cryst.* A**35**, 789–795.
Moroney, L. M., Thompson, P. & Cox, D. E. (1988). *J. Appl. Cryst.* **21**, 206–208.
Noma, T., Yoshimura, M., Somiya, S., Kato, M., Shibata, M. & Seto, H. (1989). *Advances in Ceramics*, Vol. 24, *Science and Technology of Zirconia III*, edited by S. Somiya, N. Yamamoto and H. Yanagida, pp. 377–384. Ohio, USA: The American Ceramics Society.
Paton, M. G. & Maslen, E. N. (1965). *Acta Cryst.* **19**, 307–310.
Sasaki, S. (1989). KEK Report 88-14, pp. 23, 59. National Laboratory for High Energy Physics, Tsukuba.
Sasaki, S. (1990). KEK Report 90-16, p. 61. National Laboratory for High Energy Physics, Tsukuba.
Satow, Y. & Iitaka, Y. (1989). *Rev. Sci. Instrum.* **60**, 2390–2393.
Smith, D. K. & Newkirk, H. W. (1965). *Acta Cryst.* **18**, 983–991.
Steele, D. & Fender, B. E. F. (1974). *J. Phys. C*, **7**, 1–11.
Suzuki, S., Tanaka, M. & Ishigame, M. (1985). *Jpn. J. Appl. Phys.* **24**, 401–410.
Suzuki, S., Tanaka, M. & Ishigame, M. (1987). *J. Phys. C*, **20**, 2963–2972.
Teo, B.-K. & Lee, P. A. (1979). *J. Am. Chem. Soc.* **101**, 2815–2832.
Tokonami, M. (1965). *Acta Cryst.* **19**, 486.
Udagawa, Y. (1993). *X-ray Absorption Fine Structure* (in Japanese), pp. 176-218. Tokyo: Gakken-Shuppan Centre.
Yamada, T., Yoshimura, M. & Somiya, S. (1986). *High Temp. High Pressures*, **18**, 377–388.
Yashima, M., Ishizawa, N. & Yoshimura, M. (1992). *J. Am. Ceram. Soc.* **75**, 1550–1557.
Yashima, M., Ohtake, K., Kakihana, M., Arashi, H. & Yoshimura, M. (1996). *J. Phys. Chem. Solids*, **57**, 17–24.
Welberry, T. R., Butler, B. D., Thompson, J. G. & Withers, R. L. (1993). *J. Solid State Chem.* **106**, 461–475.
Welberry, T. R., Withers, R. L., Thompson, J. G. & Butler, B. D. (1992). *J. Solid State Chem.* **100**, 71–89.